Journal of Physics D: Applied Physics

PAPER • **OPEN ACCESS**

Ultra-broadband THz absorbers based on 3D graphene

To cite this article: Prabhat Kumar *et al* 2023 *J. Phys. D: Appl. Phys.* **56** 505103

View the article online for updates and enhancements.

You may also like

- Metal-assisted-chemical-etching of silicon nanowires for templating 3D graphene growth towards energy storage in microsystems
Jinhua Li, Nguyen Van Toan, Zhuqing Wang et al.
- Dual-layer graphene based tunable broadband terahertz absorber relying on the coexistence of hybridization and stacking effects
Rong Lin, Xiaoliang He, Zhilong Jiang et al.
- Advances in research on 2D and 3D graphene-based supercapacitors
Johannes Ph. Mensing, Chatwarin Poochai, Sadanan Kerdpocha et al.

This content was downloaded from IP address 147.231.19.34 on 24/10/2023 at 19:05

OPEN ACCESS
IOP Publishing
Journal of Physics D: Applied Physics
J. Phys. D: Appl. Phys. **56** (2023) 505103 (7pp)
https://doi.org/10.1088/1361-6463/acfb1c

Ultra-broadband THz absorbers based on 3D graphene

Prabhat Kumar[1], Martin Šilhavík[1], Jiří Červenka[1] and Petr Kužel[2,*]

[1] Department of Thin Films and Nanostructures, Institute of Physics of the Czech Academy of Sciences, Cukrovarnická 10/112, Prague 162 00, Czech Republic
[2] Department of Dielectrics, Institute of Physics of the Czech Academy of Sciences, Na Slovance 2, Prague 8 18221, Czech Republic

E-mail: kuzelp@fzu.cz

Received 25 July 2023, revised 8 September 2023
Accepted for publication 19 September 2023
Published 28 September 2023

Abstract

We use terahertz and multi-terahertz spectroscopy to investigate optical properties of three-dimensional (3D) graphene across a wide frequency range of 0.15–10 THz. We explore the electromagnetic shielding, stealth, and absorber capabilities of 3D graphene samples annealed at various temperatures up to 1300 °C. We show that the tradeoff between the transmitted, absorbed and reflected power of the materials can be controlled by the annealing temperature through a fine broadband tuning of the refractive and absorptive indices of the material. This ultralight system (with a specific mass of $\sim 7\,\mathrm{mg\,cm^{-3}}$) is capable of acting as a stealth element (non-annealed sample, $R < 1\%$), THz absorber (annealing at 750 °C, $A > 85\%$) or a shielding coating (annealing at 1300 °C, $T < 0.1\%$) within an ultrabroadband range of 0.2–7 THz. All these properties can be combined by stacking these materials on top of each other, which provides unique opportunities for THz applications.

Supplementary material for this article is available online

Keywords: absorbers, terahertz, 3D graphene

(Some figures may appear in colour only in the online journal)

1. Introduction

Terahertz (THz) electromagnetic waves provide a promising and unexplored bandwidth bridging the gap between the current electronic and photonic devices. The THz technology thus holds novel potential for significant advancements in various fields such as communications (6G) [1], security [2–4], imaging [5, 6], and spectroscopy [7, 8]. However, harnessing the full potential of THz radiation requires efficient control and manipulation of these waves. Significant progress has been achieved in the development of terahertz sources [9, 10] and detectors [11]. Currently, an urgent need arises for highly efficient and tunable THz absorbers for thermal detectors, radar systems, electromagnetic shielding, and other THz applications.

To address this need, extensive research was launched to explore materials that can absorb THz radiation across a wide bandwidth without undesired reflection. Previous approaches have involved mostly metamaterials exhibiting antireflective properties and absorption resonances (thus narrow-band operation) [12–15]. Some of the proposed metamaterials structures have also featured multilayer graphene sheets [16–18]. High-porosity three-dimensional (3D) graphene materials have been demonstrated to exhibit excellent wide-angle absorbing properties in the range below 1 THz [19]. However, 3D graphene has not yet been well explored at the higher THz frequencies.

* Author to whom any correspondence should be addressed.

Original content from this work may be used under the terms of the Creative Commons Attribution 4.0 licence. Any further distribution of this work must maintain attribution to the author(s) and the title of the work, journal citation and DOI.

© 2023 The Author(s). Published by IOP Publishing Ltd

Carbon-based materials have garnered considerable attention recently due to their structure-dependent interaction with THz radiation [20–22]. For example, graphite (hybridization sp^2) is a good electrical conductor with the THz absorption coefficient $\alpha \sim 1.3 \times 10^3\,cm^{-1}$ and the refractive index $n \sim 16$, whereas the diamond (hybridization sp^3) is an insulator with $\alpha \sim 0.05\,cm^{-1}$ and $n \sim 2.3$ in the THz range [20–22]. The discovery of graphene (a single layer of sp^2-bonded carbon atoms) and an advancement in its synthesis process led, among others, to the production of 3D porous structures, generally called graphene aerogels (GA) or 3D graphene foams [23, 24]. 3D graphene materials have recently demonstrated highly attractive properties for applications in the THz range [25]. In this structure, the THz-related properties can be tuned by the C–C covalent cross-linking between the graphene flakes [23] and chemical functionalization [26]. Previous studies have reported promising absorption properties of 3D graphene in the THz range, spanning from 0.1 to 1.2 THz [19]. Other investigations have explored the modulation of THz waves using graphene foam through electric and optical field excitation within the 0.2–1.6 THz range [27].

Recently, we have shown that a relaxational mechanism dominates the charge carrier transport in 3D graphene networks [26]. The response of 3D graphene to the THz excitation consists of an interplay between the carrier hopping among localized states and a band-like (Drude) contribution of free carriers. These contributions can be controlled by changing the number of defects in the materials using a simple thermal annealing process [26]. High-temperature annealing can heal defects and improve the electrical conductivity of complex 3D graphene samples, leading to an increasing contribution of the Drude term. This process can also be used for tuning the optical properties of 3D graphene in the THz range.

In this work, we determine the optical properties of 3D graphene foams in an ultrabroad range of 0.15–10 THz. Our study evaluates the transmission, reflection, and absorption properties of various samples, either non-annealed (i.e. reduced graphene-oxide networks) or annealed 3D graphene foams at 400 °C–1300 °C. We comprehensively examine these properties with the aim to find optimum conditions for electromagnetic shielding, stealth, and absorber layers over the whole THz range. Our study reveals that the THz properties of the samples can be effectively tuned between the stealth and shielding behavior by means of the annealing temperature. Both of these properties can be combined in a single structure using a stack of differently annealed 3D graphene samples, which opens up new opportunities for THz applications within the ultra-broadband spectral range.

2. Experimental section

2.1. Synthesis of 3D graphene

Sixty milligram of graphene oxide (GO) in powder (XFNANO) was mixed with 30 ml of deionized water. GO solution was delicately mixed with hand and immersed in an ultrasonic bath. The solution was sonicated for 60 min at a temperature kept in the range of 30 °C–40 °C. The GO mixture was transferred into a Teflon-lined hydrothermal stainless-steel autoclave with a volume of 50 ml and annealed in an oven at 180 °C for 6 h. After the hydrothermal process, a reduced and self-assembled 3D GO hydrogel structure was obtained. The hydrogel was washed with deionized water multiple times to remove the residuals and freeze-dried at −70 °C in vacuum (2×10^{-1} mBar) for 16 h to get a stable reduced graphene oxide (rGO) aerogel in the form of a cylinder. The obtained rGO sample (denoted as non-annealed) was then annealed in a custom-made furnace at different temperatures, i.e. 400 °C, 750 °C, and 1300 °C, to produce a 3D GA. The sample annealing affected the GA composition by removing the oxygen-related functional groups [28]. The content of C reached almost ∼100% after the annealing at 1300 °C. A scheme of the fabrication process is depicted in supplementary material (figure S1). The samples measured in this work are different specimens than those reported in our previous paper [26]; however, the fabrication procedure was nominally the same.

2.2. Material characterization

Scanning electron microscopy (TESCAN MAIA3) was used to characterize the morphology of the GO and annealed GA samples. The samples were also measured by x-ray photoelectron spectroscopy (XPS Kratos Analytical Ltd) and Raman spectroscopy (Renishaw inVia setup using a 442 nm laser). The compositional analysis of the samples stemming from XPS measurements has shown similar results to the GA materials presented in our previous work [26], see figure S2 in supplementary material. 3D graphene materials exhibit long-term stability in ambient air and maintain their properties over time. Given that these materials are primarily composed of graphene, they share comparable sensitivities to external factors as their 2D graphene counterparts [29–32].

2.3. THz spectroscopy

A conventional femtosecond oscillator-based time-domain THz spectroscopy setup [33] and a femtosecond amplifier-based multi-THz spectroscopy setup (2-color plasma rectification/ABCD detection [34]) were used to measure the transmittance of the samples under normal incidence in the 0.15–10 THz spectral range. The schemes of both experiments are also shown in the supplementary material, figure S3. The thicknesses of the samples used for spectroscopic measurements were adjusted by mechanical polishing to obtain good quality transmittance data (from ∼ 0.75 mm for the relatively transparent non-annealed sample down to ∼ 0.23 mm for the relatively opaque sample annealed at 1300 °C) and they were determined using an Olympus optical microscope.

3. Results and discussion

THz optical spectra of the GA samples annealed at different temperatures are shown in figure 1. The spectra were calculated from the measured complex transmission functions

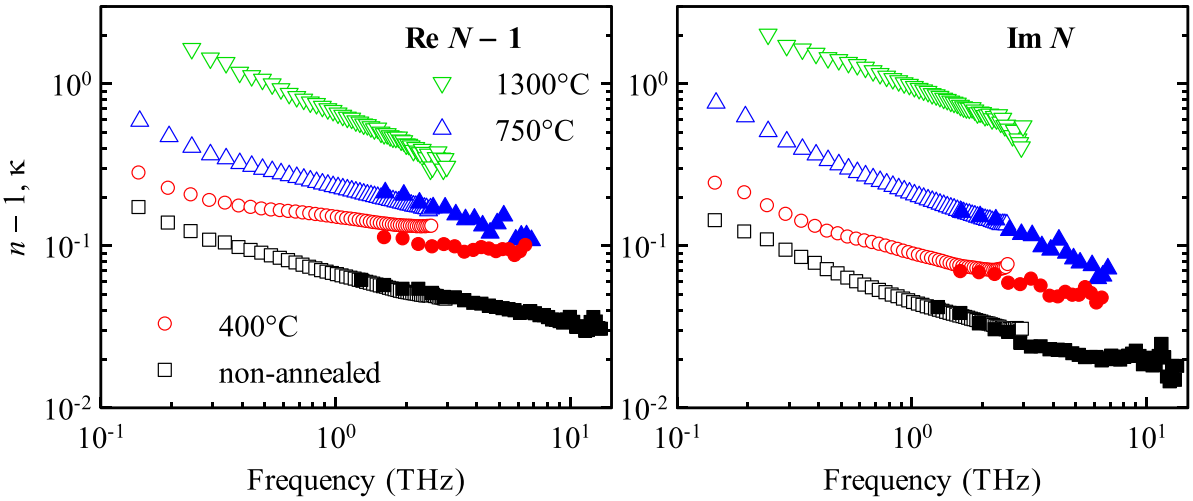

Figure 1. Refractive (n) and absorptive (κ) indices of the studied samples measured by THz (open symbols) and multi-THz (closed symbols) spectroscopies. We plot $n-1$ (left panel) and κ (right panel) in the log scales in order to emphasize the variation of properties among the samples.

in the THz and multi-THz range (figure S4 in supplementary material) including the Gouy shift correction following equation (S1) in the supplementary material and a description in [33]. Since the pores inside the samples are at most μm-sized and thus largely sub-wavelength (the wavelength of radiation at 10 THz corresponds to 30 μm), the samples behave as an effective medium for THz radiation and can be well described by a frequency dependent effective complex refractive index $N = n + i\kappa$. We observe a good match between the results of the two employed experimental setups, except for a small difference in the refractive index of the sample annealed at 400 °C, which is most probably caused by a spatially inhomogeneous thickness of the sample, as it was manually thinned down for the measurements. These spectra thus represent intrinsic material properties and can be used for further calculations of various optical quantities like absorptivity, transmissivity and reflectivity.

The spectra in figure 1 indicate that the refractive (n) and absorptive (κ) indices of the samples vary significantly as a function of the annealing temperature: both n and κ grow with the increasing annealing temperature. The obtained THz properties are in line with those published in our previous paper [26], where we investigated the transport mechanisms occurring in 3D graphene. We observed increasing conductivity and decreasing permittivity with frequency due to a complex interplay between the carrier hopping among localized states and a Drude contribution of conduction-band carriers.

The optical properties of the GA samples were evaluated using the measured THz spectra of the complex refractive indices. Power transmissivity $T(\omega)$ and power reflectivity $R(\omega)$ were calculated from Fresnel equations applied to a slab of 3D graphene material (see, e.g. [35], for general formulae). Power absorptivity $A(\omega)$ was calculated as:

$$A(\omega) = 1 - R(\omega) - T(\omega). \tag{1}$$

The absorptivity curves determined from the experimental data for all the samples are shown in figure 2. The selected transmissivity and reflectivity curves are depicted in figures 3(a)–(d). We show only $T(\omega)$ and $R(\omega)$ spectra which are important for the overall behavior of the samples, i.e. their values are essentially larger than $\sim 2\%$. The ensemble of all the evaluated data is shown in supplementary material (figure S5).

We observe that for the non-annealed sample and for the sample annealed at 400 °C the absorptivity spectra strongly depend on the material thickness. Indeed, in this case, samples behave like a weakly conductive semi-transparent foam with a refractive index close to 1 and an absorptive index close to zero. The dominant term at the right-hand side of equation (1) is $T(\omega)$, which depends on the sample thickness due to the weak absorption of the material, see figures 3(a) and (b). The reflectivity is small, and one finds $R(\omega) \lesssim 2\%$ in the investigated range (see supplementary material, figure S5). Therefore, the sample exhibits suitable properties for stealth applications.

For samples annealed at higher temperatures, the absorptivity is practically thickness independent. This is because of the increased refractive and absorptive indices, which lead to an increased impedance mismatch between the air and the samples and thus to a significantly higher reflectivity. For the sample annealed at 1300 °C the reflectivity largely dominates at the right-hand side of equation (1), see figures 2 and 3(d), and virtually no radiation is transmitted ($< 1\%$). This material thus presents a high electromagnetic interference shielding efficiency (EMI SE $= -10 \log T$). The specific shielding efficiency (*SSE*) can be expressed as [36]:

$$\mathrm{SSE} = -\frac{10 \log T}{\rho d}, \tag{2}$$

where d is the shielding slab thickness and ρ is its specific mass ($\rho \approx 6 - 8\,\mathrm{mg\,cm^{-3}}$ in our samples). We find

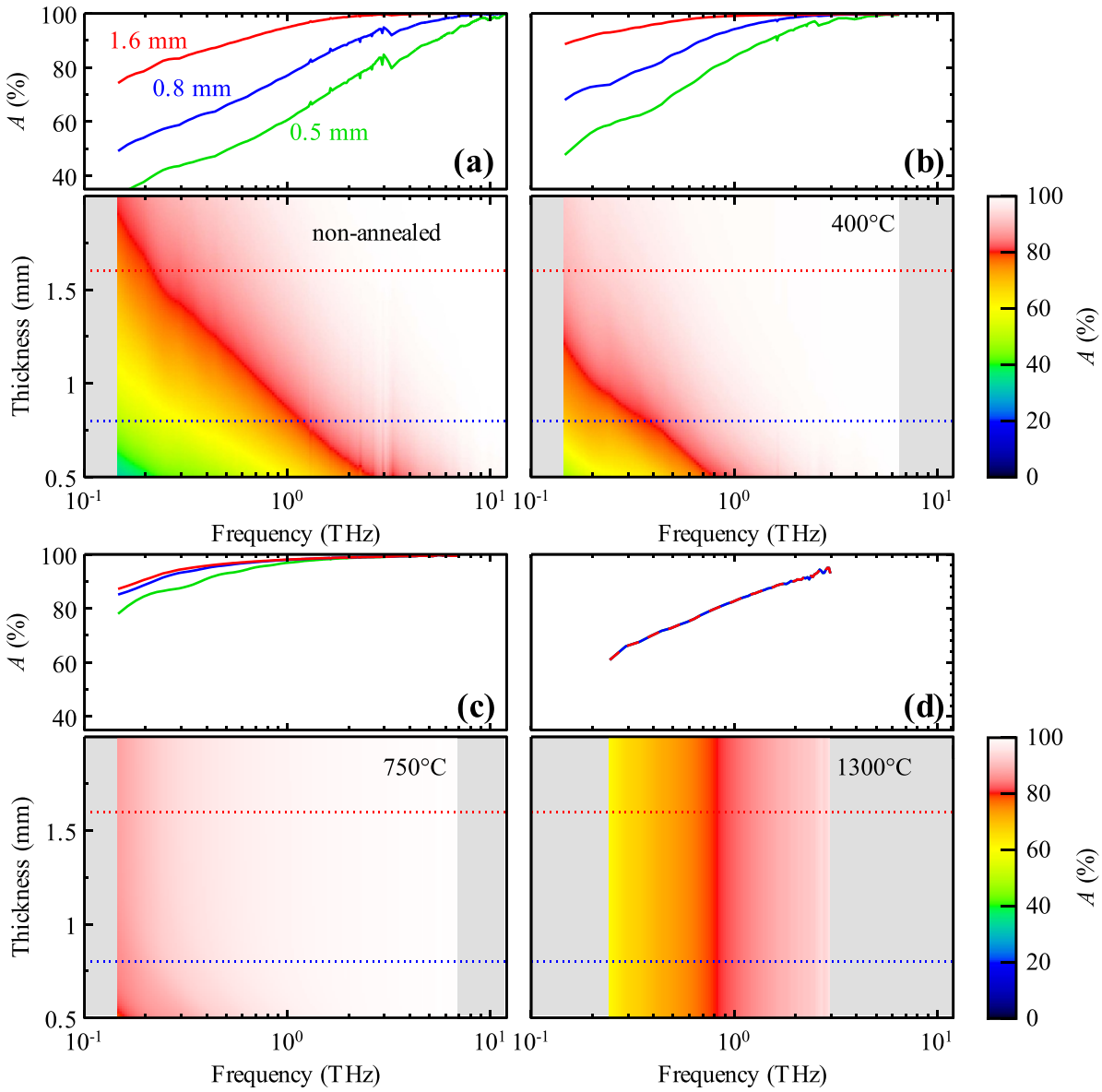

Figure 2. Absorptivity of variously annealed 3D graphene samples as a function of frequency and sample thickness, which was calculated from the measured optical data in the THz range (figure 1). The colormap plots (bottom plots for each sample) display continuous variation of the sample thickness; the gray parts represent frequency intervals where the experimental data are not available. The top plots represent the absorptivity for three selected thicknesses (corresponding to horizontal cuts of the colormaps at 0.5, 0.8 and 1.6 mm).

that the GA sample annealed at 1300 °C has SSE $\approx 2.5 \times 10^5$ dB cm^2 g^{-1} at 1 THz. This material thus demonstrates a high *EMI SE* and *SSE* and can be used for preventing disruptive signals from entering a sensitive area of THz devices and in aerospace devices where the weight is pertinent.

For the sample annealed at 750 °C, figures 2 and 3(c), the reflectivity and transmissivity are approximately balanced, reaching about 10% at 0.15 THz for a 0.5 mm thick slab and decreasing towards higher frequencies. This balanced behavior leads to the best performance in terms of the absorbed power, which exceeds 80% of the incident power from 0.15 THz up to 7 THz. The observed balanced reflectivity and transmissivity are due to a proper interplay between a moderately small conductivity (i.e. moderately low absorptive index) and a small permittivity (or refractive index), which is close to unity and minimizes the impedance mismatch.

The annealing temperature thus significantly affects the THz optical properties of 3D graphene materials. An increase in the annealing temperature leads to an increased electrical conductivity (both static and dynamic [26]). This is due to the removal of the oxygen-related function groups from the reduced 3D graphene structure and due to a healing of the structural defects in the 3D graphene structure [26]. The tradeoff between the transmitted, absorbed and reflected power is physically adjusted by the ratio of the carbon and oxygen in the system and by the amount of sp^2 domains formed during the annealing temperature. These processes provide a unique playground for tuning the optical properties of 3D graphene in the THz and multi-THz range.

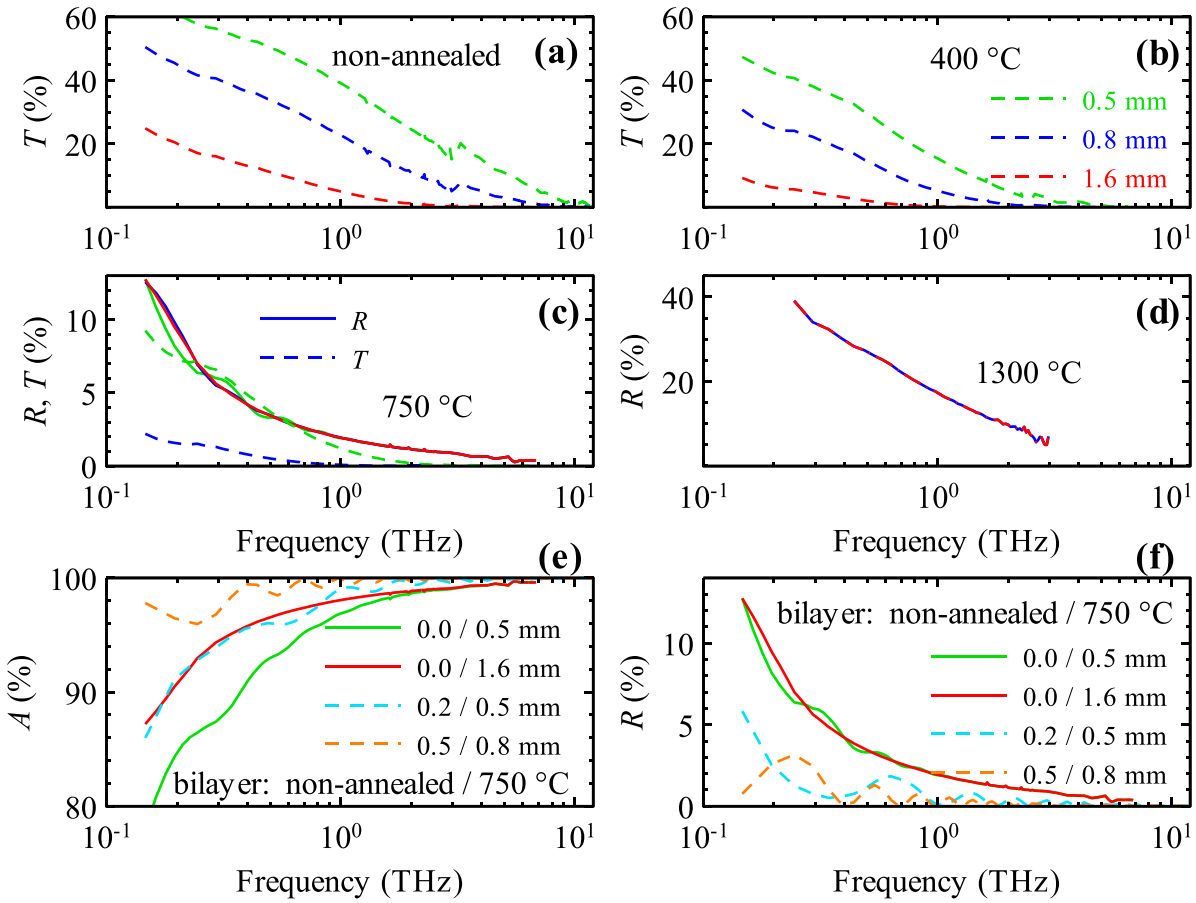

Figure 3. (a)–(d) Transmissivity and reflectivity of the variously annealed 3D graphene materials evaluated for several slab thicknesses (0.5, 0.8 and 1.6 mm). (e) Absorptivity and (f) reflectivity of bilayers composed of a non-annealed layer and a layer annealed at 750 °C. The legend indicates the respective thicknesses of the two layers. Solid lines are shown for comparison and correspond to a single layer annealed at 750 °C.

An interesting possibility consists in stacking variously annealed materials to build a more complex (layered) sample. Indeed, the stacking can be mechanically accomplished very easily due to the remarkable mechanical stability and elastic properties of 3D graphene [23]. With a minimum amount of stress, the two layers can be put into optical contact without any air gap and without a significant change of THz properties. An example of optical properties of a selected bilayer structure is shown in figures 3(e) and (f). Here we combine a thinner non-annealed layer and a thicker layer annealed at 750 °C. On the one hand, the transmissivity of such a bilayer (not shown in figure 3) is somewhat lower (but still comparable) to the transmissivity of a single layer annealed at 750 °C. This is because the non-annealed component is relatively transparent (figure 3(a)). On the other hand, the non-annealed layer exhibits an excellent impedance matching with the surrounding air, and its presence thus leads to a significant decrease of the reflection losses of the bilayer in comparison with a single layer annealed at 750 °C (figure 3(f)). This behavior then leads to a significant increase in the total absorptivity of the structure. We observe in figure 3(e) that $A(\omega)$ exceeds 96% in the whole investigated spectral range for the bilayer composed of a 0.5 mm thick non-annealed layer and of a 0.8 mm thick layer annealed at 750 °C. Such a structure then acts simultaneously as a stealth, shielding and absorber element over a spectral range well exceeding one decade in frequency.

4. Conclusion

We have shown that 3D graphene foams exhibit intriguing optical properties in the THz and multi-THz range. These materials enable a control over shielding, absorbing and stealth properties by adjusting the number of oxygen species attached to the graphene lattice using a simple annealing process. This process enables to finely tune the refractive index of the 3D graphene slightly above the value for the air while adjusting the absorptive index, which causes absorption of electromagnetic energy within a penetration depth of the order of the wavelength or somewhat shorter (i.e., in the sub-millimeter range). In particular, we observed that the sample annealed at 1300 °C has suitable properties for EMI shielding. The non-annealed sample demonstrates interesting properties for stealth applications. We also show that the sample annealed at 750 °C exhibits high absorption and low reflection over a wide THz range, opening new avenues for highly efficient

ultra-broadband THz absorbers. Most importantly, an optical element composed of a bilayer of variously annealed materials can act simultaneously as a stealth, shielding and absorber element over a spectral range well exceeding one decade in frequency.

Data availability statement

The data that support the findings of this study are available upon reasonable request from the authors.

Acknowledgments

P Kumar would like to thank the support from the Czech Academy of Sciences under the Programme to Support Prospective Human Resources. We also acknowledge the financial support from the Czech Science Foundation (Project No. 19-28375X) and from Operational Programme Research, Development and Education financed by European Structural and Investment Funds and the Czech Ministry of Education, Youth and Sports (Projects No. CZ.02.1.01/0.0/0.0/16_019/0000760).

ORCID iDs

Jiří Červenka https://orcid.org/0000-0002-1873-2475
Petr Kužel https://orcid.org/0000-0003-1134-9198

References

[1] Nagatsuma T, Ducournau G and Renaud C C 2016 Advances in terahertz communications accelerated by photonics *Nat. Photon.* **10** 371–9
[2] Ma J, Shrestha R, Adelberg J, Yeh C-Y, Hossain Z, Knightly E, Jornet J M and Mittleman D M 2018 Security and eavesdropping in terahertz wireless links *Nature* **563** 89–93
[3] Kemp M C, Taday P F, Cole B E, Cluff J A, Fitzgerald A J and Tribe W R 2003 Security applications of terahertz technology *Proc. SPIE* **5070** 44
[4] Troha T, Ostatnický T and Kužel P 2021 Improving security in terahertz wireless links using beam symmetry of vortex and Gaussian beams *Opt. Express* **29** 30461
[5] Wen Y, Jia D, Ma W, Feng Y, Liu M, Dong L, Zhao Y and Yu X 2017 Photomechanical meta-molecule array for real-time terahertz imaging *Microsyst. Nanoeng.* **3** 17071
[6] Castro-Camus E, Koch M and Mittleman D M 2022 Recent advances in terahertz imaging: 1999–2021 *Appl. Phys.* B **128** 12
[7] Beard M C, Turner G M and Schmuttenmaer C A 2002 Terahertz spectroscopy *J. Phys. Chem.* B **106** 7146–59
[8] Peiponen K-E, Zeitler A and Kuwata-Gonokami M 2013 *Terahertz Spectroscopy and Imaging* vol 171 (Springer)
[9] Ferguson B and Zhang X-C 2002 Materials for terahertz science and technology *Nat. Mater.* **1** 26–33
[10] Lewis R A 2014 A review of terahertz sources *J. Phys. D: Appl. Phys.* **47** 374001
[11] Lewis R A 2019 A review of terahertz detectors *J. Phys. D: Appl. Phys.* **52** 433001
[12] Tao H, Landy N I, Bingham C M, Zhang X, Averitt R D and Padilla W J 2008 A metamaterial absorber for the terahertz regime: design, fabrication and characterization *Opt. Express* **16** 7181
[13] Shen S, Liu X, Shen Y, Qu J, Pickwell-macpherson E, Wei X and Sun Y 2022 Recent advances in the development of materials for terahertz metamaterial sensing *Adv. Opt. Mater.* **10** 2101008
[14] Shen Z, Li S, Xu Y, Yin W, Zhang L and Chen X 2021 Three-dimensional printed ultrabroadband terahertz metamaterial absorbers *Phys. Rev. Appl.* **16** 014066
[15] Liu M *et al* 2017 Ultrathin tunable terahertz absorber based on MEMS-driven metamaterial *Microsyst. Nanoeng.* **3** 17033
[16] Masyukov M S and Grebenchukov A N 2021 Temporally modulated metamaterial based on a multilayer graphene structure *Phys. Rev.* B **104** 165308
[17] Nefedov I S, Valagiannopoulos C A and Melnikov L A 2013 Perfect absorption in graphene multilayers *J. Opt.* **15** 114003
[18] Masyukov M, Grebenchukov A N, Litvinov E A, Baldycheva A, Vozianova A V and Khodzitsky M K 2020 Photo-tunable terahertz absorber based on intercalated few-layer graphene *J. Opt.* **22** 095105
[19] Huang Z *et al* 2018 Ultra-broadband wide-angle terahertz absorption properties of 3D graphene foam *Adv. Funct. Mater.* **28** 1704363
[20] Gusakov P E, Andrianov A V, Aleshin A N, Matsushita S and Akagi K 2012 Electrical and optical properties of doped helical polyacetylene graphite films in terahertz frequency range *Synth. Met.* **162** 1846–51
[21] Afsar M N and Chi H 1994 Window materials for high power gyrotron *Int. J. Infrared Millim. Waves* **15** 1161–79
[22] Venkatachalam S, Zeranska-Chudek K, Zdrojek M and Hourlier D 2020 Carbon-based terahertz absorbers: materials, applications, and perspectives *Nano Sel.* **1** 471–90
[23] Šilhavík M, Kumar P, Zafar Z A, Míšek M, Čičala M, Piliarik M and Červenka J 2022 Anomalous elasticity and damping in covalently cross-linked graphene aerogels *Commun. Phys.* **5** 27
[24] Luo S, Samad Y A, Chan V and Liao K 2019 Cellular graphene: fabrication, mechanical properties, and strain-sensing applications *Matter* **1** 1148–202
[25] Chen H, Ma W, Huang Z, Zhang Y, Huang Y and Chen Y 2019 Graphene-based materials toward microwave and terahertz absorbing stealth technologies *Adv. Opt. Mater.* **7** 1801318
[26] Kumar P, Šilhavík M, Parida M R, Němec H, Červenka J and Kužel P 2023 Terahertz charge transport dynamics in 3D graphene networks with localization and band regimes *Nanoscale Adv.* **5** 2933–40
[27] Xu S, Fan F, Cheng J, Chen H, Ma W, Huang Y and Chang S 2019 Active terahertz shielding and absorption based on graphene foam modulated by electric and optical field excitation *Adv. Opt. Mater.* **7** 1900555
[28] Kumar P, Šilhavík M, Zafar Z A and Červenka J 2023 Universal strategy for reversing aging and defects in graphene oxide for highly conductive graphene aerogels *J. Phys. Chem.* C **127** 10599–608
[29] Wang X, Sun Y and Liu K 2019 Chemical and structural stability of 2D layered materials *2D Mater.* **6** 042001
[30] Ye N, Wang Z, Wang S, Fang H and Wang D 2018 Aqueous aggregation and stability of graphene nanoplatelets, graphene oxide, and reduced graphene oxide in simulated natural environmental conditions: complex roles of surface and solution chemistry *Environ. Sci. Pollut. Res.* **25** 10956–65
[31] Xing W, Lalwani G, Rusakova I and Sitharaman B 2014 Degradation of graphene by hydrogen peroxide *Part. Part. Syst. Charact.* **31** 745–50

[32] Singha Roy S, Safron N S, Wu M-Y and Arnold M S 2015 Evolution, kinetics, energetics, and environmental factors of graphene degradation on silicon dioxide *Nanoscale* **7** 6093–103
[33] Kužel P, Němec H, Kadlec F and Kadlec C 2010 Gouy shift correction for highly accurate refractive index retrieval in time-domain terahertz spectroscopy *Opt. Express* **18** 15338
[34] Skoromets V, Němec H, Goian V, Kamba S and Kužel P 2018 Performance comparison of time-domain terahertz, multi-terahertz, and Fourier transform infrared spectroscopies *J. Infrared Millim. Terahertz Waves* **39** 1249–63
[35] Born M and Wolf E 2003 *Basic Properties of the Electromagnetic Field in Principles of Optics* 7th edn (University Press, Cambridge) pp 64–67
[36] Li G, Amer N, Hafez H A, Huang S, Turchinovich D, Mochalin V N, Hegmann F A and Titova L V 2020 Dynamical control over terahertz electromagnetic interference shielding with 2D $Ti_3C_2T_y$ MXene by ultrafast optical pulses *Nano Lett.* **20** 636–43